Electrostatics-driven shape transitions in soft shells

Vikram Jadhao[a], Creighton K. Thomas[a], and Monica Olvera de la Cruz[a,b,c,d,1]

Departments of [a]Materials Science and Engineering, [b]Chemistry, [c]Chemical and Biological Engineering, and [d]Physics, Northwestern University, Evanston, IL 60208

Contributed by Monica Olvera de la Cruz, July 25, 2014 (sent for review March 25, 2014)

Manipulating the shape of nanoscale objects in a controllable fashion is at the heart of designing materials that act as building blocks for self-assembly or serve as targeted drug delivery carriers. Inducing shape deformations by controlling external parameters is also an important way of designing biomimetic membranes. In this paper, we demonstrate that electrostatics can be used as a tool to manipulate the shape of soft, closed membranes by tuning environmental conditions such as the electrolyte concentration in the medium. Using a molecular dynamics-based simulated annealing procedure, we investigate charged elastic shells that do not exchange material with their environment, such as elastic membranes formed in emulsions or synthetic nanocontainers. We find that by decreasing the salt concentration or increasing the total charge on the shell's surface, the spherical symmetry is broken, leading to the formation of ellipsoids, discs, and bowls. Shape changes are accompanied by a significant lowering of the electrostatic energy and a rise in the surface area of the shell. To substantiate our simulation findings, we show analytically that a uniformly charged disc has a lower Coulomb energy than a sphere of the same volume. Further, we test the robustness of our results by including the effects of charge renormalization in the analysis of the shape transitions and find the latter to be feasible for a wide range of shell volume fractions.

elasticity | long-range interactions | morphology | nanotechnology

Biological matter in cells is often compartmentalized by elastic membranes that take various shapes such as blood cell membranes, organelles, and viral capsids. These biomembranes are highly optimized to perform specific functions. A key focus of current biomedical technologies is to engineer synthetic materials that can match the performance and structural sophistication displayed by natural entities. Mimicking key physical features of biomembranes, including shape, size, and flexibility, is a crucial step toward the design of such synthetic biomaterials (1). Recent findings also indicate that the shape of a drug-carrier nanoparticle directly influences the amount and efficiency of drug delivery (2–5). The shape and deformability of soft materials such as colloids, emulsions, hydrogels, or micelles play an important role in determining their usefulness in various technological applications as well (6–9). For example, colloidal self-assembly is governed to a large extent by the shape of individual colloids (6, 10, 11). Similarly, controlling the shape and size of reverse micelles is of key importance in their use as solvent extraction systems for removing rare earth metals from aqueous solutions or as templates for nanoparticle synthesis (12–15).

Shape transformations in materials are engineered via chemically induced modifications (10, 11) or using techniques such as photoswitching of membrane properties (16) and controlled evaporation of the enclosed solvent (17). However, generating desired material shapes with precision and manipulating them with relative ease at the nanoscale has been a challenge (6). From the theoretical standpoint, much attention has been focused on finding the low-energy conformations of flexible materials, modeled often as soft elastic membranes, in the hope of suggesting superior experimental systems that can enable the design of nanostructures (18–20). Examples include the exploration of shape transitions driven by topological defects (21–23) or compression (24), and the study of low-energy conformations of multicomponent shells (18, 25–27).

Changing the shape of an elastic shell entails bending and stretching it, and the associated energy costs form the components of the elastic free energy of the shell (28). However, when the shell is charged, it is possible to compensate for the increase in elastic energy associated with the shape deformation if the latter is accompanied with a significant lowering of the electrostatic free energy (29–33). Previous studies on charged soft membranes mainly focused on mapping a charged elastic shell to an uncharged elastic shell with charge-renormalized elastic parameters (34–39). In the case of charged nanoshells, electrostatic screening length is comparable to the shell dimensions, and the surface-charge density can assume high values. As a result, shell models where Coulomb interactions are included explicitly are needed (29, 30). Using such models, it has been shown that an ionic shell, where positive and negative charges populate the surface, lowers its energy by taking an icosahedral shape with the same surface area (29). In this work, we find that a uniformly charged, spherical elastic shell, when constrained to maintain the enclosed volume, can lower its free energy by deforming into smooth structures such as ellipsoids, discs, and bowls (Fig. 1). We show that the transition to these nonspherical shapes can be driven by varying environmental properties such as the electrolyte concentration in the surrounding solvent.

To include the nonlinear coupling between the shape of the shell and its electrostatic response self-consistently, we study the charged soft nanoshells numerically. We model the charged shell by a set of discrete points placed on a spherical membrane, forming a mesh consisting of vertices, edges, and faces (Fig. S1), recognizing that in the limit of large number of vertices the discretized elastic membrane recovers the physics of the associated continuum model (see *Materials and Methods* for details). The uniform surface-charge density is simulated by assigning every vertex with the same charge. We work with elastic parameters such that the uncharged shell assumes a spherical

Significance

Shape is a fundamental property of an object that influences its interaction with the environment and often determines the object's functional capabilities. Understanding how to generate and control shape by modifying the environmental conditions is of primary importance in designing systems that respond to external cues. We show here that electrostatic interactions can be used to change the equilibrium shape of soft, nanometer-sized shells. We find that a uniformly charged, spherical shell undergoes shape changes, transforming into ellipsoids, discs, and bowls, as the electrolyte concentration in the environment is decreased. This electrostatics-based shape design mechanism, regulated by varying properties external to the shell, can be used to build efficient nanocontainers for various medical and technological applications.

Author contributions: V.J., C.K.T., and M.O.d.l.C. designed research; V.J. and C.K.T. performed research; V.J., C.K.T., and M.O.d.l.C. analyzed data; and V.J., C.K.T., and M.O.d.l.C. wrote the paper.

The authors declare no conflict of interest.

[1]To whom correspondence should be addressed. Email: m-olvera@northwestern.edu.

This article contains supporting information online at www.pnas.org/lookup/suppl/doi:10.1073/pnas.1413986111/-/DCSupplemental.

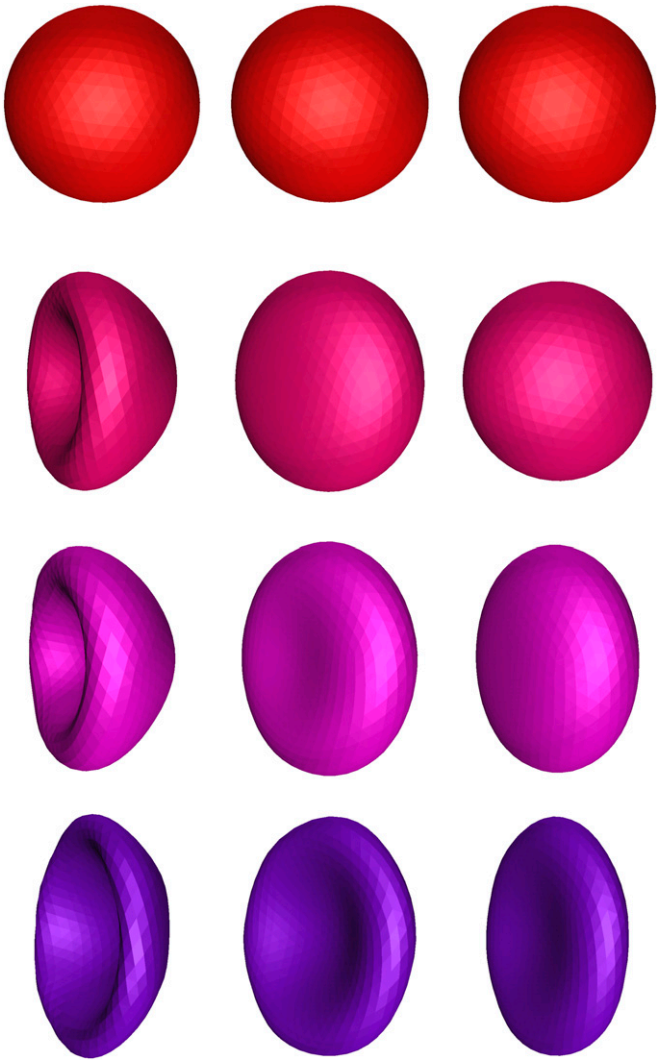

Fig. 1. Snapshots of minimum-energy conformations of charged elastic nanoshells for three different bending rigidities κ = 1, 5, and 10 (columns from left to right). In each column the electrolyte concentration c (M) decreases (rows from top to bottom) as c = 1, 0.1, 0.05, and 0.005. Different colors suggest different concentration values, with red being the highest c under study and purple corresponding to the lowest c. As the concentration is lowered, the range of electrostatic interactions is increased, leading to the variation in the shape of the nanoshell. We find that for the concentration range under investigation, softer shells tend to form bowl-like structures, wheras more rigid vesicles form ellipsoidal and disc-like shapes. All of the above nanostructures have the same total surface charge and volume, fixed to values associated with the spherical conformation.

shape at equilibrium. We allow only the deformations that preserve the shell's total volume, the latter being chosen to be that of the uncharged conformation. Our model is applicable to monolayers, such as emulsions or reverse micelles where nanodroplets of oil or water are surrounded by properly polymerized charged surfactant molecules, and also to incompressible bilayer systems and nanocontainers that do not exchange material with their environment. In the following sections, we provide evidence that this minimum model reproduces various shapes observed experimentally. Furthermore, we test the validity of this electrostatic model and associated simulation results by providing analytical solutions in limiting cases, namely by computing the electrostatic energy of oblate spheroidal shells and comparing it with that of a sphere of the same volume in salt-free conditions. Effects of ion condensation are then included via a two-state model to derive the renormalized charge on the spherical and spheroidal shells to test the robustness of our results.

Using the discretization of the continuum expression for the elastic energy introduced in ref. 21, we write the free energy $\mathcal{F}$ associated with the discretized shell as

$$\mathcal{F}\left[\{\mathbf{r}_i\}\right] = \frac{\kappa}{2}\sum_{l\in \mathrm{E}} \left|\mathbf{n}_{l,1} - \mathbf{n}_{l,2}\right|^2 + \frac{k}{2R^2}\sum_{l\in \mathrm{E}} \left(\left|\mathbf{r}_{l,1} - \mathbf{r}_{l,2}\right| - a_l\right)^2 + \frac{l_B z^2}{2}\sum_{i,j\in \mathrm{V}} \frac{e^{\frac{-\left|\mathbf{r}_i - \mathbf{r}_j\right|}{\lambda_\mathrm{D}}}}{\left|\mathbf{r}_i - \mathbf{r}_j\right|}, \quad [1]$$

where $\mathcal{F}$ is measured in units of k_BT. Here T is the room temperature and k_B is the Boltzmann constant. We make the free energy dimensionless by defining $\kappa = \tilde{\kappa}/k_BT$, where $\tilde{\kappa}$ is proportional to the bending rigidity κ_b of the continuum model, and $k = \tilde{k}R^2/k_BT$, with $\tilde{k}$ being proportional to the 2D Young's modulus Y of the continuous elastic membrane, and R is the spherical shell radius. We use the dimensionless bending rigidity κ and the spring constant k as the scale for bending and stretching energies respectively. In Eq. **1**, E and V denote the set of all edges and vertices respectively, and $\mathbf{r}_i$ is the position vector of the ith vertex. The first term on the right-hand side is the bending energy with $\mathbf{n}_{l,1}$ and $\mathbf{n}_{l,2}$ being the normal vectors to the faces adjacent to edge l. The second term is the stretching energy with $\mathbf{r}_{l,1}$ and $\mathbf{r}_{l,2}$ being the position vectors of the vertices corresponding to the edge l, and a_l is the rest length of edge l. The last term is the (dimensionless) electrostatic energy of the model membrane. We consider an aqueous environment inhabiting electrolyte whose presence is taken into consideration implicitly, leading to screened Coulomb interactions between each vertex pair. Here, l_B denotes the Bjerrum length in water, λ_D is the Debye length, and z is a dimensionless charge associated with each vertex. We assume a uniform dielectric to simplify the computations, thus ignoring any induced charge effects.

As is evident from Eq. **1**, the free energy $\mathcal{F}$ is a function of the set of vertex position vectors $\{\mathbf{r}_i\}$ which also parametrizes the shape of the shell. The equilibrium shape of the shell is the one that corresponds to the minimum of $\mathcal{F}$ subject to constraint of fixed enclosed volume. We perform this constrained free-energy minimization using a molecular dynamics (MD)-based simulated annealing procedure, details of which are provided in *Materials and Methods*.

Results

The uncharged elastic shell conformation in all our simulations is a sphere of radius $R \approx 10$ nm. We discretize the sphere with $N \approx 1{,}000$ points, generating a nearly uniform distribution with an average edge length of $a \approx 1$ nm. We fix the elastic spring constant $k = 100$ in all simulations. This value corresponds to $Y = 1$ k_BT per nm^2 which, for the bending rigidities under investigation, leads to shells characterized by a Föppl–von Kármán number (YR^2/κ) in the range of 10 to 100. We consider a monovalent electrolyte with concentration c. The Debye length λ_D is known via the relation $\lambda_\mathrm{D} = 0.304/\sqrt{c}$ nm (40). The concentration c thus parametrizes the spatial range of Coulomb interactions. In our simulations, we tune c such that this range varies from $\lambda_D < a$, in which case the shell mimics the behavior of an uncharged elastic shell, to $\lambda_D \approx R$, which corresponds to the case where most charges feel each other.

In Fig. 1, we show the change in the shape corresponding to the minimum of the shell free energy $\mathcal{F}$ as c is varied. Here, we set $z = 0.6$, which is equivalent to a shell surface potential of ~100 mV. Each column represents the shapes obtained for a fixed value of κ, with the latter increasing from left to right assuming the values κ = 1, 5, and 10. Within each column, c decreases from top to bottom as c = 1, 0.1, 0.05, and 0.005 M. This range of concentration covers most biological and synthetic

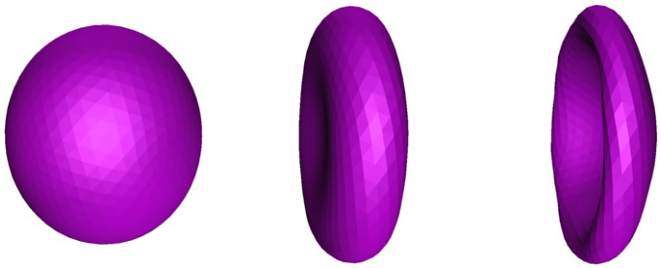

Fig. 2. Shell shapes that minimize free energy $\mathcal{F}$ for fixed $\kappa = 5$ and $c = 0.015$ M as a function of increasing $z = 0.3$, 0.6, and 1 (from left to right). As z increases, the strength of the electrostatic interactions increase and the shell transforms from a convex, ellipsoidal form to a dimpled disc and finally to a concave bowl-like structure. All shapes correspond to the same total volume. See *Results* for the meaning of symbols.

conditions. We see that the top row ($c = 1$ M) comprises spherical shapes. At $c = 1$ M, the screening length is very small ($\lambda_D < a$) and hence the electrostatic forces only come into effect at extremely short distances, resulting in a nearly vanishing contribution to the overall free energy. This leads to conformations that resemble the shape of the uncharged elastic shell, which is spherical. However, as c is lowered, transitions to a variety of nonspherical shapes are observed.

In case of the most flexible charged shell (Fig. 1, left column), increasing the range of the electrostatic interactions leads to the formation of concave structures, hereafter referred to as bowls. The opening of the bowl widens with decreasing c. For a shell with a higher bending rigidity (center column), as c is lowered, the shell first assumes a convex, ellipsoidal shape; then a biconcave, disc-like structure; and finally the shell deforms into a bowl. We note the similarity between the biconcave discs we obtain and the shape of synthetic red blood cells (1), despite the differences in their respective physical origins and sizes. The right column shows the results for the most rigid membrane under study. Due to the high-energy penalty associated with bending, the shell remains spherical even at $c = 0.1$ M. However, upon further lowering of c, we first witness an ellipsoidal shape and then a flattened disc-like structure at $c = 0.005$ M. It is worth noting that the discs and bowls we obtain closely resemble the shapes of elastic structures in ref. 16 that are synthesized using light as a tool to engineer shape.

Next, we study the effects of modulating the strength of Coulomb interactions on shell shape. In Fig. 2 we show snapshots of minimum-energy shell conformations when we vary the parameter z keeping the flexibility of the shell and the salt concentration in the environment constant ($\kappa = 5$ and $c = 0.015$ M). Changing z corresponds to simulating shells with different total charge on the surface. The shapes from left to right correspond to the values of $z = 0.3$, 0.6, and 1. We find that at $z = 0.3$, the shell assumes a convex ellipsoidal shape. As z is increased to 0.6, the ellipsoid deforms into a dimpled disc; and finally at $z = 1$, the bowl structure is obtained.

The transition to nonspherical shapes is accompanied by a decrease in the electrostatic energy. In the upper half of Fig. 3, we plot ΔE_C, the total Coulomb energy of the final structure relative to that of the spherical shell with identical parameters. The data for ΔE_C is shown as a function of c for various values of $z = 0.3$, 0.6, and 1 and $\kappa = 1$ and 10. In all cases, ΔE_C is negative. For convex shapes (spheres and ellipsoids)—represented by black symbols—ΔE_C is small. On the other hand, for discs and bowls—represented by blue and red symbols, respectively—the reduction in electrostatic energy is more pronounced. In general, as the concentration c is lowered, the behavior of ΔE_C suggests that the spherical shell deforms to an ellipsoid, then to a disc, and finally to a bowl. We find that the nonspherical shapes have a larger surface area relative to the spherical conformation (lower half in Fig. 3). We expect this to be the case as for a given fixed volume, a sphere has the lowest surface area. We find in some cases, the minimum-energy structure has twice the surface area of a sphere with same volume. Although a more general model of the elastic shell would include an energy penalty associated with increasing the surface area, we expect the shape changes to occur in situations where the surface energy increase due to the rise in area is compensated by the adsorption of molecules (such as neutral surfactants) to the membrane, thereby reducing its surface tension. Using the data in Fig. 3 we estimate that the shell surface tension should be low, $\mathcal{O}(1)$ dyne per cm, for the aforementioned predicted shapes to be realized.

In Fig. 4, we show the distribution of local electrostatic and elastic energies on the disc (upper two rows) and bowl (lower two rows). The disc corresponds to the case of $z = 0.6$, $\kappa = 10$, and $c = 0.005$ M and the bowl shape is characterized by $z = 0.6$, $\kappa = 1$, and $c = 0.1$ M. The electrostatic energy at a vertex is computed by summing over the screened Coulomb interactions of the charge at that vertex with all other charges on the shell. As the scale bars on the right point out, the electrostatic energy is the dominant of the two energies and drives the shape formation, with the elastic energy adapting locally to conform to the new shape. For both disc and bowl, the local elastic energy (second and fourth rows) has large spatial variations and tends to be higher on the more bent regions of the nanoshell. For the disc shape, the Coulomb energy (first row) is higher near the center. This is, in part, due to the enhanced repulsion resulting from the proximity of the opposite faces which are at a distance less than the Debye length associated with this system.

Discussion

Increasing the range or strength of electrostatic interactions enhances the Coulomb repulsion between any two charged vertices, making them move apart. However, the resulting extension in edge lengths is penalized by the rise in the stretching energy. In addition, the bending energy term penalizes any sharp changes in curvature, thus favoring transitions to smooth shapes. This

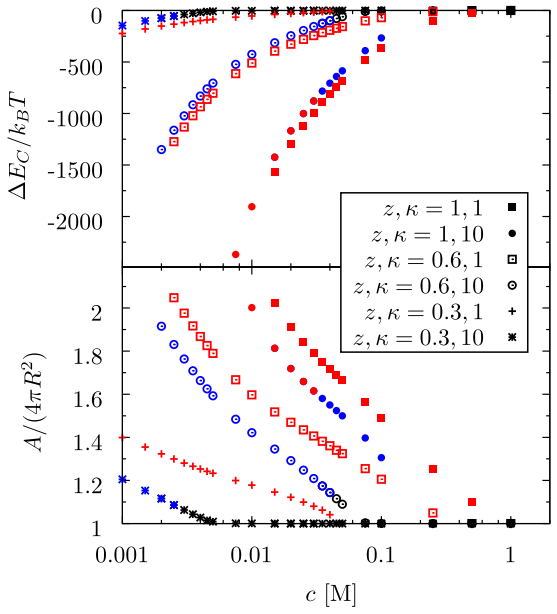

Fig. 3. Electrostatic contribution to the energy of the shell (upper plot) and shell's surface area (lower plot) vs. salt concentration c for different lowest-energy structures. We plot the electrostatic energy, $\Delta E_C = E_C - E_{C,S}$, which is measured relative to that of a spherical shell with identical parameters. Similarly, the area A of the shell is normalized by the area of a sphere with the same volume. Black symbols are spheres or ellipsoids, blue symbols are discs, and red symbols are bowl-shaped structures. *Inset* shows the legend for the symbols used in the plot. The large (negative) changes in Coulomb energy help drive the shape transitions.

competition between the electrostatic and elastic energies sets an effective area for the nanomembrane which, in conjunction with the fixed-volume constraint, determines the eventual shape of the nanoshell. Varying the screening length or the total charge on the shell changes this effective area, leading to variations in the shell shape.

To substantiate the above explanation, we focus on the sphere-to-ellipsoid-to-disc part of the observed shape transitions and perform analytical calculations. Judging by the simulation snapshots (see the images in the right column of Fig. 1), these shapes can be approximated as oblate spheroids with different degrees of eccentricity e and major semiaxis lengths a. Because the volume of the shell is fixed, the oblate spheroidal shell can be characterized by a single parameter e. For $e \to 0$, one obtains sphere-like shapes and $e \to 1$ leads to disc-like conformations. The competition between elastic and electrostatic energies can now be considered as determining the eccentricity e for the oblate spheroid. The concentration c is seen as the control over e such that the lowering of c can be understood as an increase in e. Thus, we can verify the order of shape transitions observed in our simulations by examining the change in the electrostatic energy of a uniformly charged shell as its eccentricity is increased.

For simplicity, we consider unscreened Coulomb interactions in the following calculations. We evaluate the electrostatic energy U of a uniformly charged oblate spheroidal shell with total surface charge zN and with volume constrained to $\Omega = (4/3)\pi R^3$ (derivation in *SI Text*). We obtain

$$U(e,z,N) = l_B \frac{z^2N^2}{2R} \frac{ie\left(1-e^2\right)^{\frac{1}{6}}}{\left(e+(1-e^2)\tanh^{-1}e\right)^2} \times \sum_{n\in\text{even}} (2n+1) P_n\left(i\frac{\sqrt{1-e^2}}{e}\right) Q_n\left(i\frac{\sqrt{1-e^2}}{e}\right) \left(I_n(e)\right)^2, \quad [2]$$

where n is an even integer, P_n and Q_n are Legendre polynomials of the first and second kind, $I_n(e) = \int_0^{\pi} \sqrt{1-e^2\sin^2 v} P_n(\cos v)\sin v\, dv$, and U is evaluated relative to the thermal energy at room temperature. We define dU as the electrostatic energy of the oblate spheroid relative to the electrostatic energy of the sphere with identical parameters. We examine the variation of dU vs. e for the parameter set associated with the transition recorded in the open blue circles of Fig. 3 and find that the Coulomb energy of an oblate spheroidal shell subject to the constraint of constant volume decreases with increasing its eccentricity (Fig. S2). In other words, a disc-shaped shell has lower Coulomb energy than a sphere of the same volume. The order of shape transitions observed in our simulations is thus backed by the above analytical result. Next, we examine the spatial distribution of the local electrostatic energy U_L on the surface of the shell (see *SI Text* for details). We find that for a spherical shell, U_L is constant everywhere. However, as the eccentricity increases, the surface distribution of electrostatic energy becomes increasingly inhomogeneous. In particular, for $e = 0.95$, which corresponds to a disc-like shape, we find U_L varies significantly on the disc surface, assuming higher values near the disc center and low magnitude near the edge of the disc (Fig. S3). It is evident from the top row of Fig. 4 that we observe this trend in our simulation results as well.

We obtain more insight into our results by exploring the low-energy conformations of a very flexible uniformly charged shell where the elastic energy can be neglected in comparison with the Coulomb energy. Equilibrium shapes of such a shell will correspond to the minimum of the total electrostatic energy. In Eq. **2**, taking the limit $e \to 1$ gives $U = 0$, which is the lowest possible value for the Coulomb energy of a uniformly charged shell. This limit corresponds to a disc-like spheroidal shell whose area approaches infinity. Further, we check that when the enclosed volume is held fixed, the Coulomb energy of a prolate spheroidal shell vanishes as well when the shell is stretched into a long and thin wire-like shape. Thus, we obtain (at least) two distinct shell shapes that correspond to the state of lowest electrostatic energy. This result suggests that in our original model system, electrostatic interactions drive the transformation in the shell shape by favoring the deformation of sphere toward disc-like shapes, whereas the elastic energies compete with the Coulomb energy to generate oblate-shaped (ellipsoidal, disc-like) structures of various eccentricities. It also appears that the elastic energy component of the free energy favors the formation of oblate shapes to prolate ones.

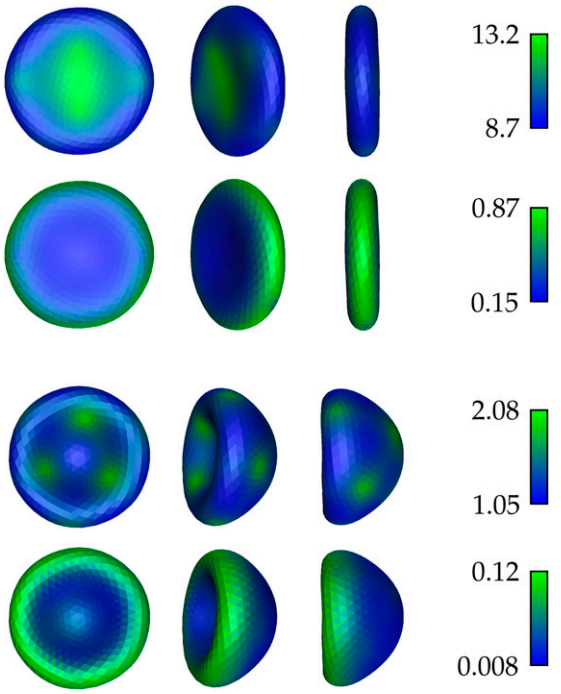

Fig. 4. Spatial distribution of electrostatic and elastic energies (in units of k_BT, where T is the room temperature) on the surface of the disc (upper two rows) and bowl (lower two rows). The left column shows the front view, the center column shows the angle view, and the right column shows the side view. For either shapes, the elastic energy (second and fourth rows) is concentrated in the edges. The electrostatic energy on the disc (first row) is higher in the center where the opposite faces are nearby. The five-coordinated vertices, which are visible as spots in the electrostatic energy distribution, lead to small fluctuations in the energy.

The constraint of fixed enclosed volume is critical to the low-energy shell conformations obtained in our simulations. If instead of the volume, the shell surface area is fixed, we expect the gallery of lowest free-energy conformations to look different from Fig. 1. We check that under the constraint of fixed area, the Coulomb energy of an oblate spheroidal shell is higher when its eccentricity increases, and the spherical shape corresponds to the conformation with the lowest Coulomb energy among all oblate shapes. However, a sphere is not the configuration that minimizes the shell electrostatic energy when prolate-shaped deformations are considered. We find that prolate spheroids of high eccentricities have lower Coulomb energy than the sphere and the lowest-energy conformation for the area-constrained system is a prolate spheroidal shell with its major axis length stretched to infinity. Hence, for the area-constrained problem, we expect the competition between Coulomb and elastic energies to give rise to different nonspherical shapes as ground-state solutions.

In our charged shell model, we assume that the counterions remain in the bulk and do not condense on the shell surface. However, in an experiment it is possible that a fraction of the counterions do condense, and in that event it becomes important to analyze their effect on the observed shape transitions. We measure this effect qualitatively in the salt-free limit for the

sphere–disc transition by using the expression for the electrostatic energy of a uniformly charged oblate shell in a two-state model of free and condensed counterions (41–43). We consider a spherically shaped Wigner–Seitz (WS) cell of volume V_{WS} with a single shell of volume $\Omega = (4/3)\pi R^3$ and surface charge zN placed at its center. We define the quantity $\eta = \Omega/V_{WS}$ as the shell volume fraction. The cell also contains N counterions, each of charge $-z$ to neutralize the shell charge. We separate the counterions into two distinct groups: free ions and condensed ions. Free ions occupy the available space in the WS cell which in the dilute limit becomes the volume of the cell. The condensed counterions are restricted to have translational motion in a thin layer of volume $V = \mathscr{A}(e,R)b$ surrounding the shell, where $\mathscr{A}(e,R)$ is the surface area of the oblate shell and $b = 1/(2\pi l_B \sigma)$ is the Gouy–Chapman length that is chosen as the condensed-layer width. Here, σ is the unrenormalized surface-charge density. When a shell has a higher σ or the system is characterized by a longer l_B, we expect the condensed-layer width to shrink owing to the enhanced counterion–shell attraction. Our choice of b as the layer thickness correctly reflects this behavior. As b is a characteristic of the charged planar surface, our analysis is limited to the regime where b is much smaller than the lengths of the major and minor semiaxis of the shell.

We write the free energy (in units of k_BT) associated with the shell in the event of ion condensation as

$$F(\alpha,e) = U\left(e,z,(1-\alpha)N\right) + \alpha N \ln\left(\frac{\alpha N\Lambda^3}{\mathscr{A}(e,R)b}\right) - \alpha N + (1-\alpha)N\ln\left(\frac{(1-\alpha)N\Lambda^3}{V_{WS}}\right) - (1-\alpha)N, \quad [3]$$

where α is the fraction of counterions that condense and Λ is the thermal de Broglie wavelength. Here, the first term is the electrostatic energy of the shell obtained from Eq. **2** by replacing zN with the reduced charge $z(1-\alpha)N$, the next two terms stem from the entropic contribution of the αN condensed ions, and the last two terms correspond to the entropy of $(1-\alpha)N$ free counterions. F can be considered as a function of two variables: eccentricity e, which characterizes the shape of the shell, and condensate fraction α, which measures the renormalized charge on the shell. For a given e, we find the condensate fraction that extremizes the above free energy F. Using α, we evaluate the equilibrium free-energy difference, dF, between the free energy of the oblate shell and that of the sphere of the same volume (see *SI Text* for details). We compute dF for the parameters associated with the transition recorded in the open blue circles of Fig. 3 and find that for all values of the volume fraction η, dF becomes increasingly more negative as the eccentricity e is raised, implying that the shape transitions from sphere to oblate spheroids are favored (Fig. S4). Additionally, we find that the condensate fraction α decreases with increasing e for all values of η. For low η, we obtain $\alpha \approx 0.1$, whereas for large η, we find the condensate fraction to be $\alpha \approx 0.5$. Regardless of the amount of condensation, we find the shell with higher eccentricity is preferred energetically.

We next examine the variation of the renormalized electrostatic energy dU with e for different η values. For low and high values of the volume fraction, we find that dU is negative and decreases, just like dF, upon the increase of the eccentricity (Fig. S5). However, for some intermediate η values, we observe that $dU > 0$, that is, the electrostatic energy increases as e is raised, in sharp contrast to the free energy associated with the shell. This suggests that for some values of shell volume fractions, the shape transitions are expected to occur despite an increase in the electrostatic energy. We attribute the feasibility of such transitions to the gain in entropy by the ions as less numbers of ions condense when the shape is deformed from a sphere to an oblate.

The main conclusions reached above remain unchanged when we repeat the two-state model analysis assuming that the shell is an equipotential surface. For all values of η, dF increasingly becomes more negative as the eccentricity e is raised, implying that the shape transitions from sphere to oblate spheroids are favored (Fig. S6). Thus, judging by the variation of dF determined by the above two-state model analysis, we conclude that the shape transitions from sphere to oblates of increasing eccentricity should be feasible in the event of ion condensation. However, due to the renormalization of the charge on the shell surface, it is likely that the specific parameter values (for example, concentration strength, bending rigidity) for which the shape transitions occur, will change. Quantitative results can be obtained by including counterions explicitly in the simulations and taking into account the induced polarization charges on the shell surface in analyzing changes in shape. We note that our MD-based simulation algorithm provides an ideal platform to include these effects via its coupling with recently introduced energy–functional-based approaches of treating dielectric inhomogeneities (44, 45).

Conclusion

We investigate the prospects of electrostatics-based generation and control of shapes in materials at the nanoscale. We find that by increasing the strength or the range of Coulomb interacting potential, a uniformly charged spherical shell, constrained to maintain its volume, deforms to structures of lower symmetry, resulting in ellipsoids, discs, and bowls. This symmetry breaking is accompanied by a reduction in the overall electrostatic energy of the shell and a significant spatial variation in the local elastic energy on the shell surface. To support our simulation findings, we show analytically that a uniformly charged disc-like spheroidal shell has a lower Coulomb energy than a spherical shell of the same volume. To evaluate the renormalization of shell charge due to nonlinear effects, we use a two-state model of free and condensed ions. We find that the shape transitions are feasible in the event of ion condensation for a wide range of shell volume fractions.

Shape changes in our model membrane are triggered by changing the attributes of the environment external to the membrane, such as the electrolyte concentration in the surrounding solvent. This is in contrast with transitions brought about by patterning the shell surface with defects (20, 22, 23) or by introducing elastic inhomogeneities on the shell surface (18, 25–27). In comparison with ionic shells (29, 30), where the primary experimental challenge is to synthesize membranes with desired stoichiometric ratios (30), our base shell surface is uniformly charged and elastically homogeneous, which is relatively simple to design.

We envision that the electrostatics-driven shell design mechanism proposed here can function as a useful template for synthesizing nanoparticle-based drug delivery carriers of desired shapes (2, 3, 5). Our results can also prove useful in the analysis of shape changes in charged emulsions or reverse micelle systems that form during the metal-extraction processes involved in the recovery of scarce rare earth elements or the cleaning of nuclear waste (15). In addition, our findings can aid in the development of theories explaining the properties of stretchable electronic materials such as dielectric elastomers where electrostatic field and deformation are intimately coupled (7, 46).

Materials and Methods

We generate the triangulation on the shell via the Caspar and Klug construction (47), which produces a lattice where each point has six neighbors with the exception of 12 five-coordinated vertices (defects). Due to the presence of these defects, the lattice has a nonvanishing initial stretching energy. We remove this residual strain by appropriately choosing rest lengths of the edges (48), leading to a vanishing stretching energy for the initial mesh. The defects, however, lead to slight variations in the surface-charge density and local elastic and electrostatic energies. By choosing a large number of lattice points, the effect of these small deviations on the resulting shape transformations is minimized. To make sure that our results are independent of the particular triangulation, we perform simulations using a sufficient number of lattice points generated via different choices of Caspar and Klug constructions, obtaining similar results for all runs.

Our lattice maintains the initial connectivity throughout the shape evolution. Because each vertex carries a charge of the same sign, our discretized

membrane is characterized with an inbuilt self-avoidance due to the mutual electrostatic repulsion between any pair of vertices. However, to ensure complete stability, we include an additional short-range, purely repulsive Lennard-Jones potential between two vertices, where each vertex is modeled as a hard sphere with radius chosen to be a fraction of the average edge length *a* associated with the triangular lattice.

We use an MD method to minimize the free energy $\mathcal{F}$, which requires the analytical expressions for the gradients of $\mathcal{F}$ with respect to the vertex positions. Evaluating the gradient of the bending energy term is relatively difficult and we show this calculation in *SI Text*. Our simulations start from a spherical shell with a nearly homogeneous surface distribution of local elastic and electrostatic energies. Slight deviations in the energies arise from the presence of five-coordinated vertices which are the result of using the aforementioned triangulation of the shell surface. We assign the vertices a kinetic energy $\mathcal{K}=\sum_i(1/2)\mu\dot{\mathbf{r}}_i^2$, and direct their motion according to the forces derived from $\mathcal{F}$, where the latter plays the role of the potential energy. We thus obtain the Lagrangian $L=\mathcal{K}-\mathcal{F}$, from which we derive the equations of motion for the vertices: $\mu\ddot{\mathbf{r}}_i=-\nabla_{\mathbf{r}_i}\mathcal{F}$. Here, μ is a mass term associated with the vertices which determines the choice of the simulation time step. These equations of motion, which form the basis of the MD simulation of the vertices, are appropriately augmented to preserve the constraint of fixed total volume. We achieve this via the Shake–Rattle routine (49) of implementing constraints that guarantees the conservation of shell volume at each simulation step. Finally, to arrive at the shape that corresponds to the minimum of the energy landscape we couple the MD scheme with simulated annealing. We associate a (fictitious) temperature with the kinetic energy of the vertices and use a Nosé–Hoover thermostat to set it. This temperature is not the physical temperature; it is merely a parameter we use to control the annealing process. We reduce this temperature at periodic intervals so as to arrive at the lowest point of the potential energy associated with the MD Lagrangian, thus reaching the minimum of the free energy $\mathcal{F}$.

ACKNOWLEDGMENTS. We thank R. Sknepnek, Z. Yao, G. Vernizzi, and J. Zwanikken for the many insightful discussions. The model was developed with the financial support of the Office of Basic Energy Sciences within Department of Energy Grant DE-FG02-08ER46539. The computational work was funded by the Office of the Director of Defense Research and Engineering and the Air Force Office of Scientific Research under Award FA9550-10-1-0167.

1. Doshi N, Zahr AS, Bhaskar S, Lahann J, Mitragotri S (2009) Red blood cell-mimicking synthetic biomaterial particles. *Proc Natl Acad Sci USA* 106(51):21495–21499.
2. Geng Y, et al. (2007) Shape effects of filaments versus spherical particles in flow and drug delivery. *Nat Nanotechnol* 2(4):249–255.
3. Barua S, et al. (2013) Particle shape enhances specificity of antibody-displaying nanoparticles. *Proc Natl Acad Sci USA* 110(9):3270–3275.
4. Kolhar P, et al. (2013) Using shape effects to target antibody-coated nanoparticles to lung and brain endothelium. *Proc Natl Acad Sci USA* 110(26):10753–8.
5. Loverde SM, Klein ML, Discher DE (2012) Nanoparticle shape improves delivery: Rational coarse grain molecular dynamics (rCG-MD) of taxol in worm-like PEG-PCL micelles. *Adv Mater* 24(28):3823–3830.
6. Cademartiri L, Bishop KJM, Snyder PW, Ozin GA (2012) Using shape for self-assembly. *Philos Trans A Math Phys Eng Sci* 370(1969):2824–2847.
7. Suo Z (2012) Mechanics of stretchable electronics and soft machines. *MRS Bull* 37(3): 218–225.
8. Hyuk Im S, Jeong U, Xia Y (2005) Polymer hollow particles with controllable holes in their surfaces. *Nat Mater* 4(9):671–675.
9. Sun Y, Mayers B, Xia Y (2003) Metal nanostructures with hollow interiors. *Adv Mater* 15(7-8):641–646.
10. Sacanna S, et al. (2013) Shaping colloids for self-assembly. *Nat Commun* 4:1688.
11. Sacanna S, Irvine WTM, Chaikin PM, Pine DJ (2010) Lock and key colloids. *Nature* 464(7288):575–578.
12. Shrestha LK, Sato T, Aramaki K (2009) Intrinsic parameters for structural variation of reverse micelles in nonionic surfactant (glycerol alpha-monolaurate)/oil systems: A SAXS study. *Phys Chem Chem Phys* 11(21):4251–4259.
13. Pileni M-P (2003) The role of soft colloidal templates in controlling the size and shape of inorganic nanocrystals. *Nat Mater* 2(3):145–150.
14. Wilson AM, et al. (2014) Solvent extraction: The coordination chemistry behind extractive metallurgy. *Chem Soc Rev* 43(1):123–134.
15. Vander Hoogerstraete T, Wellens S, Verachtert K, Binnemans K (2013) Removal of transition metals from rare earths by solvent extraction with an undiluted phosphonium ionic liquid: Separations relevant to rare-earth magnet recycling. *Green Chem* 15(4):919–927.
16. Hamada T, Sugimoto R, Vestergaard MC, Nagasaki T, Takagi M (2010) Membrane disk and sphere: Controllable mesoscopic structures for the capture and release of a targeted object. *J Am Chem Soc* 132(30):10528–10532.
17. Quilliet C, Zoldesi C, Riera C, van Blaaderen A, Imhof A (2008) Anisotropic colloids through non-trivial buckling. *Eur Phys J E Soft Matter* 27(1):13–20.
18. Vernizzi G, Sknepnek R, Olvera de la Cruz M (2011) Platonic and Archimedean geometries in multicomponent elastic membranes. *Proc Natl Acad Sci USA* 108(11):4292–4296.
19. Bowick MJ, Travesset A (2001) The statistical mechanics of membranes. *Phys Rep* 344(4-6):255–308.
20. Yong EH, Nelson DR, Mahadevan L (2013) Elastic platonic shells. *Phys Rev Lett* 111(17): 177801.
21. Seung HS, Nelson DR (1988) Defects in flexible membranes with crystalline order. *Phys Rev A* 38(2):1005–1018.
22. Lidmar J, Mirny L, Nelson DR (2003) Virus shapes and buckling transitions in spherical shells. *Phys Rev E Stat Nonlin Soft Matter Phys* 68(5 Pt 1):051910.
23. Šiber A (2006) Buckling transition in icosahedral shells subjected to volume conservation constraint and pressure: Relations to virus maturation. *Phys Rev E Stat Nonlin Soft Matter Phys* 73(6 Pt 1):061915.
24. Vliegenthart GA, Gompper G (2011) Compression, crumpling and collapse of spherical shells and capsules. *New J Phys* 13(4):045020.
25. Datta SS, et al. (2012) Delayed buckling and guided folding of inhomogeneous capsules. *Phys Rev Lett* 109(13):134302.
26. Sknepnek R, Vernizzi G, Olvera de la Cruz M (2012) Buckling of multicomponent elastic shells with line tension. *Soft Matter* 8(3):636–644.
27. Funkhouser CM, et al. (2013) Mechanical model of blebbing in nuclear lamin meshworks. *Proc Natl Acad Sci USA* 110(9):3248–3253.
28. Landau LD, Lifshitz EM (1995) *Theory of Elasticity* (Butterworth-Heinemann, London), 3rd Ed.
29. Vernizzi G, Olvera de la Cruz M (2007) Faceting ionic shells into icosahedra via electrostatics. *Proc Natl Acad Sci USA* 104(47):18382–18386.
30. Sknepnek R, Vernizzi G, de la Cruz MO (2011) Shape change of nanocontainers via a reversible ionic buckling. *Phys Rev Lett* 106(21):215504.
31. Grohn F (2010) Soft matter nanoparticles with various shapes and functionalities can form through electrostatic self-assembly. *Soft Matter* 6(18):4296–4302.
32. Leung C-Y, et al. (2012) Molecular crystallization controlled by pH regulates mesoscopic membrane morphology. *ACS Nano* 6(12):10901–10909.
33. Vorobyov I, Bekker B, Allen TW (2010) Electrostatics of deformable lipid membranes. *Biophys J* 98(12):2904–2913.
34. Winterhalter M, Helfrich W (1988) Effect of surface charge on the curvature elasticity of membranes. *J Phys Chem* 92(24):6865–6867.
35. Duplantier B, Goldstein RE, Romero-Rochn V, Pesci AI (1990) Geometrical and topological aspects of electric double layers near curved surfaces. *Phys Rev Lett* 65(4):508–511.
36. Lau AWC, Pincus P (1998) Charge-fluctuation-induced nonanalytic bending rigidity. *Phys Rev Lett* 81(6):1338–1341.
37. Kim YW, Sung W (2002) Effects of charge and its fluctuation on membrane undulation and stability. *EPL* 58(1):147.
38. Fleck CC, Netz RR (2005) Counterion density profiles at charged flexible membranes. *Phys Rev Lett* 95(12):128101.
39. Andelman D (1995) Electrostatic properties of membranes: The Poisson-Boltzmann theory. *Handbook of Biological Physics* (North-Holland, Amsterdam) Vol 1, pp 603–642.
40. Israelachvili J (2011) *Intermolecular and Surface Forces: Intermolecular and Surface Forces* (Elsevier Science, Amsterdam), Revised 3rd Ed.
41. Alexander S, et al. (1984) Charge renormalization, osmotic pressure, and bulk modulus of colloidal crystals: Theory. *J Chem Phys* 80(11):5776–5781.
42. González-Mozuelos P, Olvera de la Cruz M (1995) Ion condensation in saltfree dilute polyelectrolyte solutions. *J Chem Phys* 103(8):3145–3157.
43. Borukhov I (2004) Charge renormalization of cylinders and spheres: Ion size effects. *J Polym Sci B Polym Phys* 42(19):3598–3615.
44. Jadhao V, Solis FJ, Olvera de la Cruz M (2012) Simulation of charged systems in heterogeneous dielectric media via a true energy functional. *Phys Rev Lett* 109(22):223905.
45. Jadhao V, Solis FJ, Olvera de la Cruz M (2013) A variational formulation of electrostatics in a medium with spatially varying dielectric permittivity. *J Chem Phys* 138(5):054119.
46. Keplinger C, et al. (2013) Stretchable, transparent, ionic conductors. *Science* 341(6149): 984–987.
47. Caspar DLD, Klug A (1962) Physical principles in the construction of regular viruses. *Cold Spring Harb Symp Quant Biol* 27:1–24.
48. Katifori E, Alben S, Cerda E, Nelson DR, Dumais J (2010) Foldable structures and the natural design of pollen grains. *Proc Natl Acad Sci USA* 107(17):7635–7639.
49. Ryckaert J-P, Ciccotti G, Berendsen HJ (1977) Numerical integration of the cartesian equations of motion of a system with constraints: Molecular dynamics of n-alkanes. *J Comput Phys* 23(3):327–341.